HAL open science

Comparison between the homogenization and the multiscale methods for the analysis of very thin compressible flow between rough surfaces

Erwan Fourt, Mihai Arghir

▶ **To cite this version:**

Erwan Fourt, Mihai Arghir. Comparison between the homogenization and the multiscale methods for the analysis of very thin compressible flow between rough surfaces. Tribology International, 2022, 165, pp.107251. 10.1016/j.triboint.2021.107251 . hal-03617204

HAL Id: hal-03617204

https://hal.science/hal-03617204v1

Submitted on 16 Oct 2023

HAL is a multi-disciplinary open access archive for the deposit and dissemination of scientific research documents, whether they are published or not. The documents may come from teaching and research institutions in France or abroad, or from public or private research centers.

L'archive ouverte pluridisciplinaire **HAL**, est destinée au dépôt et à la diffusion de documents scientifiques de niveau recherche, publiés ou non, émanant des établissements d'enseignement et de recherche français ou étrangers, des laboratoires publics ou privés.

Distributed under a Creative Commons Attribution - NonCommercial 4.0 International License

Version of Record: https://www.sciencedirect.com/science/article/pii/S0301679X21003996
Manuscript_d439d087006efe2f881fc9d767cd86f1

Comparison between the homogenization and the multiscale methods for the analysis of very thin compressible flow between rough surfaces

Erwan FOURT, Mihai ARGHIR

Institut PPRIME, UPR CNRS 3346, Université de Poitiers, ISAE ENSMA

11 Bd. Pierre et Marie Curie, Bât H1, 86962 Futuroscope Chasseneuil, France

erwan.fourt@univ-poitiers.fr, mihai.arghir@univ-poitiers.fr

Abstract

The present work presents a comparison between the homogenization and the multiscale methods applied to the compressible Reynolds equation with irregular coefficients. The equation models a very thin compressible flow between rough surfaces. If the use of the homogenization method for the Reynolds equation with irregular coefficients is not new, it is for the multiscale method. Indeed, this last approach is borrowed from the flows in porous media (where only flows due to the pressure gradients are present) and is here extended to also take into account the Couette terms. The paper presents the detailed development of both methods and underlines similitudes and differences. Illustrative results obtained for a realistic geometry show the impact of the coarse mesh, the precision of the solution on the fine mesh and the computational effort of both methods compared to the original compressible Reynolds equation. Both methods worked well and the results show that they are reliable and efficient tools for the compressible Reynolds equation with irregular coefficients.

Keywords: homogenization method, multiscale method, compressible Reynolds equation, irregular coefficients

Introduction

The present work is focused on two methods (homogenization or two-scale method and the multiscale method) that should systematically be used for the analysis of thin film rough surface flows. One of the parameters conventionally accepted for delimiting the friction regimes is the dimensionless thin film thickness [1]. This parameter is defined as the ratio between the mean thin film height, h_m and the combined standard deviation of the two surfaces, σ_{eq}. This is a very simple parameter resulting from a model which considers that one of the two surfaces is smooth while the other carries all the roughness. Combining the roughness of the two surfaces is strictly correct only when both have a normal distribution of roughness heights but the model is tacitly applied for all situations [*2*]. Its advantage is not only the simplicity but also discarding unsteady effects that would naturally appear when a rough surface moves relative to another closely spaced rough surface.

It is generally accepted that for a dimensionless mean film thickness $h_m/\sigma_{eq} < 1$, the probability of sporadic contacts between surface asperities is greater than 95%. On the other hand, for $h_m/\sigma_{eq} > 3$, the probability of sporadic contacts between asperities is less than 5%, meaning there is no contact between the two surfaces. However, the surfaces roughness or texture will impact the thin film pressure up to $h_m/\sigma_{eq} = 7 \dots 10$.

© 2021 published by Elsevier. This manuscript is made available under the CC BY NC user license
https://creativecommons.org/licenses/by-nc/4.0/

The present work is focused on the last operating conditions, i.e. $3 \leq h_m/\sigma_{eq} \leq 7 \ldots 10$ and on the case of a compressible lubricant which separates the two surfaces. For an incompressible lubricant, the models used for calculating the pressure field are either the Reynolds equation corrected with flow factors or the homogenized Reynolds equation. The flow factors were introduced by Patir and Cheng [*3*] years ago and were calculated from heuristic assumptions. They represent a very convenient way of taking roughness into account because any kind of solver of the Reynolds equation can be easily adapted. However, the approach lacks a rigorous mathematical foundation.

A model with a strong mathematical background is the homogenized Reynolds equation. Bayada and Chambat [*4*] were among the first to introduce this approach for an incompressible thin film flow. They were followed by Almqvist et al. [5], [6] and Fatu and Bonneau [7]. The two last references discussed not only the homogenization of the incompressible Reynolds equation but also compared its results with the approach based on the flow factors introduced in [3]. The conclusions were that the flow factors were a rarely a satisfactory approach because they discard cross-coupling flow effects. Moreover, the original flow factors are deduced for an isotropic roughness with a normal height distribution and no control over its power spectrum.

Jai et al. [8], [9] extended the homogenization method to compressible flows with rarefaction effects while Almqvist and [10] applied it to liquid lubricants characterized by a finite isothermal compressibility modulus.

As underlined in [11], the homogenization of the Reynolds equation is a “disruptive approach”. However, it requires simplifying assumptions. It is supposed that the local thin film flow is governed by two, well separated length scales. The long scale is the length of the contact while the small scale is linked to the roughness pattern. Moreover, the roughness pattern is periodic and characterized by a small wavelength. In many cases, regular sinusoidal roughness patterns are used for validating the numerical solution of the homogenized Reynolds equation. These roughness patterns are artificial unless they do not mimic a textured surface.

The discussion can go further by recognizing that a third length scale is present in any rough lubricated contact, i.e. the minimum film thickness. For smooth surfaces, the use of the Reynolds equation is conditioned by a ratio of 10^{-3} between the minimum film thickness and the contact length. For rough surfaces, the ratio between the minimum film thickness and the roughness wavelength can only be larger than 10^{-3}; if the ratio is larger than 10^{-2} the Reynolds equation must be replaced by Stokes model [12]. However, the latter approach is mathematically more complex.

The necessary conditions for the homogenization of the Reynolds equation can appear very severe for surfaces with real roughness that don’t have a clear distinction between length scales nor a net periodic pattern. However, the homogenized Reynolds equation was applied for the analysis of general surfaces [*6*], [7]. One argument was that the autocorrelation length of the film thickness was one order of magnitude less than the length scale of the domain of analysis, therefore a periodicity pattern of roughness could be invoked. Nevertheless, the assumption of clearly separated length scales in the homogenized model is still in the background.

A different approach of the problem that doesn’t require the above mentioned simplifying assumptions is the multiscale method. This method is based on an approximation of the roughness height details on a fine grid and on their projection on a coarse grid. From this standpoint, the approach is similar to the homogenization method with a net separation of the domain and roughness length scales. However, in the multiscale method, all length scales are implicitly modeled and periodicity assumptions in the short length scale are not needed. The method is borrowed from porous media flow with irregular permeability ([13] - [15]). Indeed, Darcy and Reynolds equations

are similar excepting the shear flow (Couette) term in the latter equation. The multiscale method is therefore adapted in the present work for taking into account this term of the Reynolds equation.

The homogenization and the multiscale methods for the compressible Reynolds equation are then presented and discussed highlighting similitudes and differences. They are applied to the calculation of the pressure in very thin air films where the roughness height is $3 \leq h_m/\sigma_{eq} \leq 7 \ldots 10$. Situations when $h_m/\sigma_{eq} \leq 3$ were not dealt with for avoiding contacts between asperities. Moreover, the scope of this work is only the Reynolds roughness regime.

The two methods are thoroughly compared for the case of a 2D inclined slider with a stationary rough surface. The thin film height has given height probability distribution, power spectrum and standard deviation. A complete solution of the Reynolds equation considering all length scales is considered the reference and serves for comparisons.

The results show the accuracy of the homogenization and of the multiscale methods on coarse grids when compared to the solution of the original Reynolds equation obtained on very fine grids. The two methods have similar precisions. The accuracy of the homogenization method when used outside of its (apparent) domain of validity is an unexpected result. The pressure field reconstructed on the fine mesh also has very good precision. Moreover, it is shown that the computational effort of the two approximate methods is much lower than that required by the resolution of the original Reynolds equation.

Résumé of the homogenization approach

The compressible Reynolds equation can be resumed as a mass conservation equation. For an ideal gas and an isothermal flow regime this writes:

$$\nabla\vec{m} = \nabla(P\vec{q}) = 0 \tag{1}$$

where $\vec{m} = P\vec{q}$, $\vec{q} = (q_x, q_y)$ and

$$q_x = -\frac{h^3}{12\mu}\frac{\partial P}{\partial x} + U\frac{h}{2} \qquad q_y = -\frac{h^3}{12\mu}\frac{\partial P}{\partial y} \tag{2}$$

This yields the dimensionless equation

$$\frac{\partial}{\partial \bar{x}}\left(\bar{P}\bar{h}^3\frac{\partial \bar{P}}{\partial \bar{x}}\right) + \frac{\partial}{\partial y}\left(\bar{P}\bar{h}^3\frac{\partial \bar{P}}{\partial \bar{y}}\right) = \Lambda\frac{\partial}{\partial \bar{x}}(\bar{P}\bar{h}) \tag{3}$$

where $\Lambda = 6\mu UL/P_a h_{min}^2$ is the compressibility number associated with the sliding speed. For simplicity, bars indicating dimensionless pressures and lengths will be discarded in the following.

The two length scales of the homogenization approach are $\boldsymbol{x}_0$ and $\varepsilon\boldsymbol{x}_1$ with ε a small parameter and $\boldsymbol{x} = (x, y)$. In a non-dimensional description of a rectangular domain of analysis , $\boldsymbol{x}_0, \boldsymbol{x}_1 \in [0,1] \times [0,1]$. The length coordinate is then:

$$\boldsymbol{x} = \boldsymbol{x}_0 + \varepsilon\boldsymbol{x}_1, \tag{4}$$

It is supposed that the pressure field follows the same description.

$$P = P_0 + \varepsilon P_1 \tag{5}$$

Replacing (4) and (5) in Reynolds equation (3) and separating the terms of order ε^{-2}, $\varepsilon^{-1}$and ε^0 yields three equations:

$$\varepsilon^{-2}:\ A_0 P_0 = 0 \tag{6}$$
$$\varepsilon^{-1}:\ A_1 P_0 + A_0 P_1 + A_0' P_0 = \Lambda\, \partial(P_0 h)/\partial x_1 \tag{7}$$
$$\varepsilon^{0}:\ A_2 P_0 + A_1 P_1 + A_1' P_0 + A_0' P_1 = \Lambda[\partial(P_0 h)/\partial x_0 + \partial(P_1 h)/\partial x_1] \tag{8}$$

Where

$$A_0 = \frac{\partial}{\partial x_1}\left(P_0 h^3 \frac{\partial}{\partial x_1}\right) + \frac{\partial}{\partial y_1}\left(P_0 h^3 \frac{\partial}{\partial y_1}\right) \tag{9}$$
$$A_1 = \frac{\partial}{\partial x_0}\left(P_0 h^3 \frac{\partial}{\partial x_1}\right) + \frac{\partial}{\partial y_0}\left(P_0 h^3 \frac{\partial}{\partial y_1}\right) + \frac{\partial}{\partial x_1}\left(P_0 h^3 \frac{\partial}{\partial x_0}\right) + \frac{\partial}{\partial y_1}\left(P_0 h^3 \frac{\partial}{\partial y_0}\right) \tag{10}$$
$$A_2 = \frac{\partial}{\partial x_0}\left(P_0 h^3 \frac{\partial}{\partial x_0}\right) + \frac{\partial}{\partial y_0}\left(P_0 h^3 \frac{\partial}{\partial y_0}\right) \tag{11}$$
$$A_0' = \frac{\partial}{\partial x_1}\left(P_1 h^3 \frac{\partial}{\partial x_1}\right) + \frac{\partial}{\partial y_1}\left(P_1 h^3 \frac{\partial}{\partial y_1}\right) \tag{12}$$
$$A_1' = \frac{\partial}{\partial x_0}\left(P_1 h^3 \frac{\partial}{\partial x_1}\right) + \frac{\partial}{\partial y_0}\left(P_1 h^3 \frac{\partial}{\partial y_1}\right) + \frac{\partial}{\partial x_1}\left(P_1 h^3 \frac{\partial}{\partial x_0}\right) + \frac{\partial}{\partial y_1}\left(P_1 h^3 \frac{\partial}{\partial y_0}\right) \tag{13}$$
$$A_2' = \frac{\partial}{\partial x_0}\left(P_1 h^3 \frac{\partial}{\partial x_0}\right) + \frac{\partial}{\partial y_0}\left(P_1 h^3 \frac{\partial}{\partial y_0}\right) \tag{14}$$

Equations (6) - (8) are defined on an elementary cell defined by $(x_1, y_1) \in \Omega = [0,1] \times [0,1]$. Equation (6) can be written as:

$$\frac{\partial}{\partial x_1}\left(h^3 \frac{\partial P_0^2}{\partial x_1}\right) + \frac{\partial}{\partial y_1}\left(h^3 \frac{\partial P_0^2}{\partial y_1}\right) = 0 \tag{15}$$

and its solution is:

$$P_0 = const. \text{ over } \Omega. \tag{16}$$

i.e. P_0 doesn't depend on x_1 and y_1. This results and the periodicity of P_1 and h over Ω permits to verify for eq. (7) that

$$\int_\Omega [A_1 P_0 + A_0 P_1 + A_0' P_0 - \Lambda\, \partial(P_0 h)/\partial x_1] dx_1 dy_1 = 0 \tag{17}$$

An equation for P_1 over the domain Ω is then obtained from eq. (7) :

$$\frac{\partial}{\partial x_1}\left(h^3 \frac{\partial P_1}{\partial x_1}\right) + \frac{\partial}{\partial y_1}\left(h^3 \frac{\partial P_1}{\partial y_1}\right) = -\frac{\partial P_0}{\partial x_0}\frac{\partial h^3}{\partial x_1} - \frac{\partial P_0}{\partial y_0}\frac{\partial h^3}{\partial y_1} + \Lambda \frac{\partial h}{\partial x_1} \tag{18}$$

with periodicity boundary conditions for P_1. This equation has the same form as for the incompressible homogenized Reynolds equation [*7*], the main reason being the solution given by eq.

(16). If this solution doesn't hold as for example in [*9*] where large Knudsen number effects were considered, then eq. (6) is non-linear and the solution follows a different path.

Equation (18) is linear, therefore P_1 can be described by terms of the same form as its right hand side:

$$P_1 = \frac{\partial P_0}{\partial x_0}\chi_1 + \frac{\partial P_0}{\partial x_0}\chi_2 + \chi_3, \chi_i = \chi_i(x_0, y_0, x_1, y_1), i = \overline{1,3} \tag{19}$$

where χ_i are Ω periodic functions. Replacing (19) in the linear eq. (18) and identifying similar terms yields three differential equations.

$$\begin{aligned} &\frac{\partial}{\partial x_1}\left(h^3\frac{\partial \chi_i}{\partial x_1}\right) + \frac{\partial}{\partial y_1}\left(h^3\frac{\partial \chi_i}{\partial y_1}\right) = RHS_i, i = \overline{1,3} \\ &RHS_1 = -\partial h^3/\partial x_1, RHS_2 = -\partial h^3/\partial y_1, RHS_3 = \partial h/\partial x_1 \end{aligned} \tag{20}$$

Finally, equation (8) is integrated over Ω and following the previous assumptions (P_1 and h are Ω periodic) and results (P_0 is constant over Ω) and yields:

$$\begin{aligned} &\frac{\partial}{\partial x_0}\left[P_0\left(\int_\Omega h^3 d\Omega\right)\frac{\partial P_0}{\partial x_0}\right] + \frac{\partial}{\partial x_0}\left[P_0\left(\int_\Omega h^3\frac{\partial P_1}{\partial x_1}d\Omega\right)\frac{\partial P_0}{\partial y_0}\right] \\ &+\frac{\partial}{\partial y_0}\left[P_0\left(\int_\Omega h^3 d\Omega\right)\frac{\partial P_0}{\partial y_0}\right] + \frac{\partial}{\partial y_0}\left[P_0\left(\int_\Omega h^3\frac{\partial P_1}{\partial y_1}d\Omega\right)\frac{\partial P_0}{\partial x_0}\right] = \Lambda\frac{\partial}{\partial x_0}\left(P_0\int_\Omega h d\Omega\right) \end{aligned} \tag{21}$$

The homogenized compressible Reynolds equation is obtained after injecting P_1 given by (19) in eq. (21).

$$\begin{aligned} &\frac{\partial}{\partial x_0}\left(P_0 A_{11}\frac{\partial P_0}{\partial x_0}\right) + \frac{\partial}{\partial x_0}\left(P_0 A_{12}\frac{\partial P_0}{\partial y_0}\right) \\ &+\frac{\partial}{\partial y_0}\left(P_0 A_{22}\frac{\partial P_0}{\partial y_0}\right) + \frac{\partial}{\partial y_0}\left(P_0 A_{21}\frac{\partial P_0}{\partial x_0}\right) + \frac{\partial}{\partial x_0}(P_0 B_1) + \frac{\partial}{\partial x_0}(P_0 B_2) = 0 \end{aligned} \tag{22}$$

and the homogenized coefficients are calculated with the solutions of eqs. (20):

$$\begin{aligned} &A_{11} = \int_\Omega h^3\left(1 + \frac{\partial \chi_1}{\partial x_1}\right)d\Omega \ , \qquad A_{12} = \int_\Omega h^3\frac{\partial \chi_2}{\partial x_1}d\Omega \\ &A_{21} = \int_\Omega h^3\frac{\partial \chi_1}{\partial y_1}d\Omega \ , \qquad A_{22} = \int_\Omega h^3\left(1 + \frac{\partial \chi_2}{\partial y_1}\right)d\Omega \\ &B_1 = \int_\Omega h^3\frac{\partial \chi_3}{\partial x_1}d\Omega - \Lambda\int_\Omega h d\Omega \ , B_2 = \int_\Omega h^3\frac{\partial \chi_3}{\partial y_1}d\Omega \end{aligned} \tag{23}$$

The homogenized compressible Reynolds equation (22) is different from eq. (3) because it contains cross coupling derivatives. For example, the homogenized mass and volume fluxes are:

$$\begin{aligned} &\dot{m}_x = P_0 q_x, q_x = A_{11}\frac{\partial P_0}{\partial x_0} + A_{12}\frac{\partial P_0}{\partial y_0} + B_1 + B_2 \\ &\dot{m}_y = P_0 q_y, q_y = A_{21}\frac{\partial P_0}{\partial x_0} + A_{22}\frac{\partial P_0}{\partial y_0} \end{aligned} \tag{24}$$

Equation (22) is solved on a coarse grid made of all macro-cells Ω of the analyzed domain while eqs. (20) are solved on fine grids discretizing every macro-cell. The most convenient discretization

(although not the single possible) is to consider the coarse grid and the fine grids as subdomains of a single fine grid. The situation is depicted in Figure 1 for a rectangular grid.

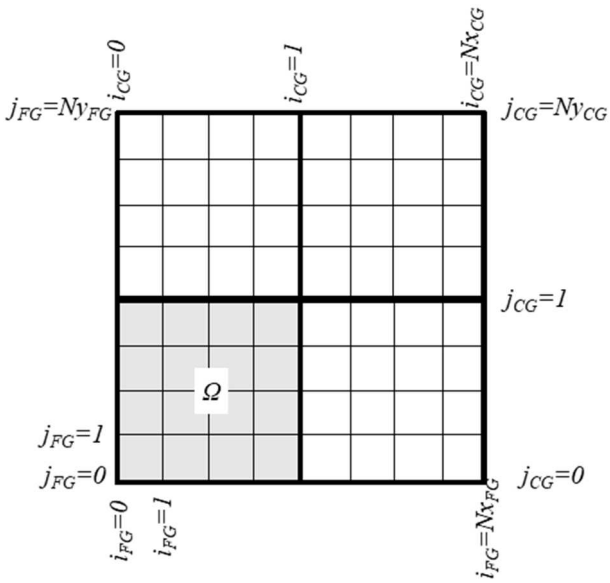

Figure 1. Coarse and fine rectangular grid discretization

Equation (22) yields a nine point stencil discretized equation for every coarse grid cell Ω when discretized with the finite volume method on a rectangular grid. The solution of this non-linear system of equations will be discussed after presenting the multiscale method.

The multiscale method

The multiscale method was introduced for the analysis of porous media flow equations with "rough" coefficients, i.e. for with rapidly varying permeability. It was first presented in the context of the finite element method [13] and then for the finite volume method [14]. The equation of porous media flow is identical with the Reynolds eq. (3) excepting the Couette mass flow rate expressed by the right hand side term. As in the homogenized method, the pressure is defined on both a coarse grid and on a fine grid but its description is different.

Following [13] and [14], the multiscale approximation of the pressure in porous media flows is based on shape functions associated with the nodes of the discretization. On a rectangular, 2D grid this yields:

$$P(\boldsymbol{x_0}, \boldsymbol{x_1}) = \sum_{i=1}^{4} P_i(\boldsymbol{x_0})\phi_i(\boldsymbol{x_0}, \boldsymbol{x_1}) \qquad (25)$$

The formula given by eq. (25) was used in [13] for three-nodes triangular finite elements and in [14] for four-nodes finite volumes. It should hold for any finite element or finite volume as long as all degrees of freedom (i.e. the number of nodes) are taken into account. A supplementary shape function will be added in the following for taking into account Couette part of the flow.

The multiscale method makes no distinction between long, short or intermediate scales. The coordinates $\boldsymbol{x_0}$ and $\boldsymbol{x_1}$ in eq. (25) identify the position on the coarse and on the fine grid, respectively, while $P_i(\boldsymbol{x_0})$ are the pressures in the nodes of the coarse grid.

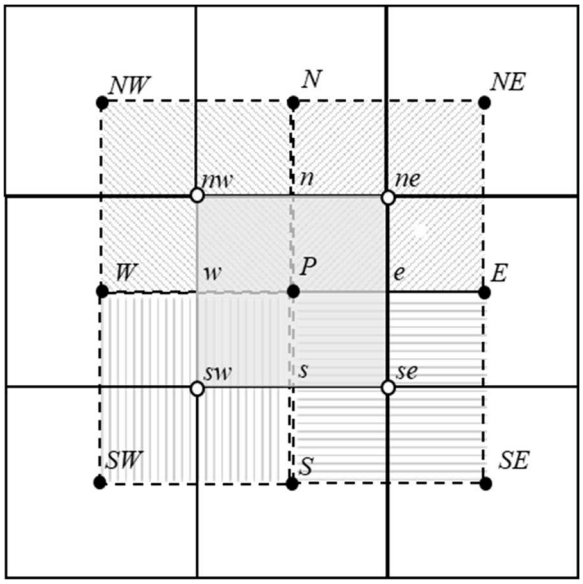

Figure 2. The basic and the dual (rectangular) coarse grid

The finite volume approach described in [14] requires two coarse grids, a basic and a dual one as depicted in Figure 2. Continuous lines indicate the basic grid and dotted lines indicate the dual grid. The centers of the basic, coarse grid are indicated by capital letters (P, E, W, etc.) while the vertices are indicated by sw, se, ne and nw.

The dual, coarse grid is x- and y-staggered relative to the basic grid. Figure 2 depicts four cells of the dual coarse grid surrounding the P-centered basic grid cell. The centers of the dual grid cells are sw, se, ne and nw.

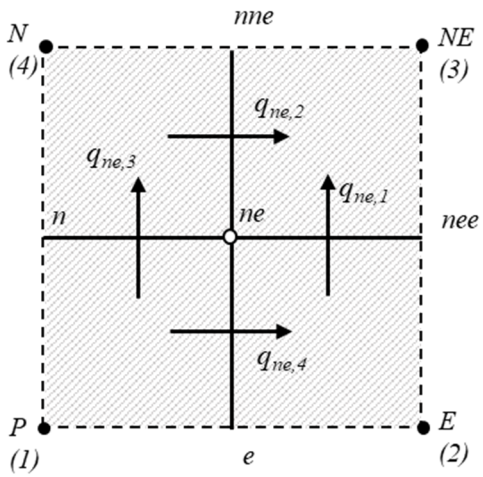

Figure 3. The ne cell of the dual coarse grid

Figure 3 details the ne-dual coarse grid cell. The approximation of the local pressure field on this cell $\hat{P}(\boldsymbol{x_0}, \boldsymbol{x_1})$ is given by eq. (25) where the indexes $i = \overline{1,4}$ are associated with P, E, NE, N, i.e. the centers of the basic coarse grid. The shape functions ϕ_i are obtained by solving four local problems on the dual coarse grid. The local problems originate from the pressure equation in porous media or from the Reynolds equation without the Couette transport term. For example, for the cell depicted in Figure 3:

$$\frac{\partial}{\partial x}\left(h^3\frac{\partial\phi_i}{\partial x}\right)+\frac{\partial}{\partial y}\left(h^3\frac{\partial\phi_i}{\partial y}\right)=0,\ x\in[x_P,x_E],\ y\in[y_P,y_N],\ i=\overline{1,4} \tag{26}$$

These equations are solved on a fine grid discretization of the dual coarse grid cell with the following boundary conditions:

$$\begin{aligned} &i=1,\phi_P=1,\phi_E=\phi_{NE}=\phi_N=0\\ &i=2,\phi_E=1,\phi_P=\phi_{NE}=\phi_N=0\\ &i=3,\phi_{NE}=1,\phi_P=\phi_E=\phi_N=0\\ &i=4,\phi_N=1,\phi_P=\phi_E=\phi_{NE}=0 \end{aligned} \tag{27}$$

It is supposed that the ϕ_i shape functions have a linear variation between successive vertices. This would imply a linear variation of the pressure between the nodes of the coarse grid and could be a rough approximation when coefficients h^3 vary very rapidly on the fine grid. Reference [14] suggests that the approximation can be improved by estimating the boundary conditions of eq. (26) from the solutions of 1D partial differential equations along the corresponding coordinate line

$$\frac{\partial}{\partial x}\left(h^3\frac{\partial\phi_i}{\partial x}\right)=0,\ \frac{\partial}{\partial y}\left(h^3\frac{\partial\phi_i}{\partial y}\right)=0 \tag{28}$$

with the boundary conditions (27). The shape functions along a boundary can then be analytically estimated; a.e. on a local fine grid with $\phi_{0,1}=\phi(x=0,1)$, $h_{0,1}=h(x=0,1)$

$$\phi(x)=\frac{\phi_0h_0^2-\phi_1h_1^2}{h_0^2-h_1^2}-\frac{(\phi_0-\phi_1)h_0^2h_1^2}{h_0^2-h_1^2}\frac{1}{h(x)^2} \tag{29}$$

The approximation described by eq. (25)-(27) based on solutions superposition is possible because the pressure equation of the incompressible flow in a porous media is linear. It can be therefore extended to the case of the Reynolds equation by adding a fifth shape function, ϕ_5.

$$\hat{P}(\boldsymbol{x_0},\boldsymbol{x_1})=\sum_{i=1}^{4}P_i(\boldsymbol{x_0})\phi_i(\boldsymbol{x_0},\boldsymbol{x_1})+\phi_5(\boldsymbol{x_0},\boldsymbol{x_1}) \tag{30}$$

This latter shape function takes into account the Couette transport term in the RHS of Reynolds equation and is the solution on the fine grid of the differential equation:

$$\frac{\partial}{\partial x}\left(h^3\frac{\partial\phi_5}{\partial x}\right)+\frac{\partial}{\partial y}\left(h^3\frac{\partial\phi_5}{\partial y}\right)=\Lambda\frac{\partial h}{\partial x} \tag{31}$$

with $\phi=0$ on all boundaries.

The approximation (30) enables then the estimation of the fluxes depicted in Figure 3:[1]

$$q_{ne/1}=\int_{x_{ne}}^{x_{nee}}\left(-h^3\frac{\partial\hat{P}}{\partial y}\right)dx=\sum_{i=1}^{4}P_iA_{ne/1,i}+A_{ne/1,5}$$

[1] A double node numbering, *i=1,2,3,4* or *i=P,E,NE,N* is used in Figure 2 and eq. (32).

$$q_{ne/2} = \int_{y_{ne}}^{y_{nne}} \left(-h^3 \frac{\partial \hat{P}}{\partial x} + \Lambda h\right) dy = \sum_{i=1}^{4} P_i A_{ne/2,i} + A_{ne/2,5}$$
$$q_{ne/3} = \int_{x_n}^{x_{ne}} \left(-h^3 \frac{\partial \hat{P}}{\partial y}\right) dx = \sum_{i=1}^{4} P_i A_{ne/3,i} + A_{ne/3,5}$$
$$q_{ne/4} = \int_{y_e}^{y_{ne}} \left(-h^3 \frac{\partial \hat{P}}{\partial x} + \Lambda h\right) dy = \sum_{i=1}^{4} P_i A_{ne/4,i} + A_{ne/4,5} \quad (32)$$

The coefficients $A_{ne/j,i}$ ($j = \overline{1,4}$ and $i = \overline{1,5}$) are detailed in the Appendix. They are calculated with the derivatives of the shape functions, $\partial\phi_i/\partial x$ and $\partial\phi_i/\partial y$ and are similar to the coefficients A_{ij} and B_i, $i,j = 1,2$ obtained in the homogenization method. This becomes more clear when writing the discretized Reynolds equation as a flux conservation equation and with the aid of Figure 4. For the incompressible Reynolds equation this yields:

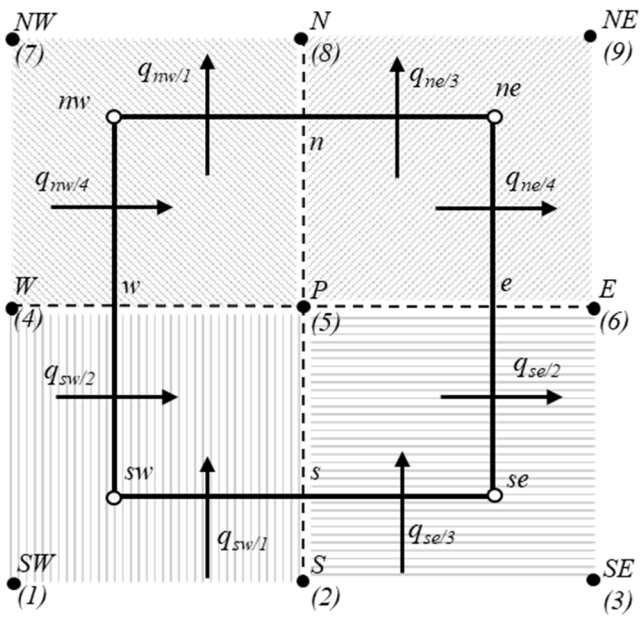

Figure 4. Flux balance on the basic coarse grid cell

$$q_{se/2} + q_{ne/4} - q_{nw/4} - q_{sw/2} + q_{ne/3} + q_{nw/1} - q_{sw/1} - q_{se/3} = 0 \quad (33)$$

The step toward the compressible Reynolds equation is straightforward. Reference [15] indicates that in the multiscale method, the approximations of the volume fluxes for the compressible Reynolds equation are the same as for the incompressible one. The explanation for this approximation is the weak variation of the pressure on a cell of the coarse mesh compared with the rest of the domain. This was rigorously proved for the homogenization method where eq. (15) and its solution (16) showed that the approximation $P_0 = const.$ holds over a cell of the coarse grid and, as a consequence, the coefficients $A_{i,j}$ and B_i, $i,j = 1,2$ used for expressing the compressible volume fluxes (24) had the same form as for the incompressible fluxes. It could be argued that eq. (15) and its solution (16) were obtained under the assumption of two different, distinct scales but the numerical results presented in this paper will show that the assumption is fully justified in a general case.

The compressible Reynolds equation approximated by the multiscale method is then:

$$P_e\left(q_{se/2}+q_{ne/4}\right)-P_w\left(q_{nw/4}+q_{sw/2}\right)+P_n\left(q_{ne/3}+q_{nw/1}\right)-P_s\left(q_{sw/1}+q_{se/3}\right)=0 \qquad (34)$$

A nine point stencil discretized equation is obtained after replacing the fluxes given by (32) in eq. (34). Again, a double node numbering, $i=1\ldots9$ or $i=SW\ldots NE$ (indicated in Figure 4) is used for simplicity.

$$\sum_{i=1}^{9} C_i P_i + D = 0 \qquad (35)$$

$$\begin{aligned}
C_1 &= -P_w A_{sw/2,SW} - P_s A_{sw/1,SW}\\
C_2 &= P_e A_{se/2,S} - P_w A_{sw/2,S} - P_s\left(A_{sw/1,S}+A_{se/3,S}\right)\\
C_3 &= P_e A_{se/2,SE} - P_s A_{se/3,SE}\\
C_4 &= -P_w\left(A_{nw/4,W}+A_{sw/2,W}\right) + P_n A_{nw/1,W} - P_s A_{sw/1,W}\\
C_5 &= P_e\left(A_{se/2,P}+A_{ne/4,P}\right) - P_w\left(A_{nw/4,P}+A_{sw/2,P}\right) + P_n\left(A_{ne/3,P}+A_{nw/1,P}\right)\\
&\quad - P_s\left(A_{sw/1,P}+A_{se/3,P}\right)\\
C_6 &= P_e\left(A_{se/2,E}+A_{ne/4,E}\right) + P_n A_{ne/3,E} - P_s A_{se/3,E}\\
C_7 &= -P_w A_{nw/4,NW} + P_n A_{nw/1,NW}\\
C_8 &= P_e A_{ne/4,N} - P_w A_{nw/4,N} + P_n\left(A_{ne/3,N}+A_{nw/1,N}\right)\\
C_9 &= P_e A_{ne/4,NE} + P_n A_{ne/3,NE}\\
D &= P_e\left(A_{se/2,5}+A_{ne/4,5}\right) - P_w\left(A_{nw/4,5}+A_{sw/2,5}\right) + P_n\left(A_{ne/3,5}+A_{nw/1,5}\right)\\
&\quad - P_s\left(A_{sw/1,5}+A_{se/3,5}\right)
\end{aligned} \qquad (36)$$

The cells of the dual grid situated on the boundaries can not be obtained by staggering the cells of the basic grid. Their size is therefore adapted in order to cover the domain of analysis as shown in Figure *5*. The discretized Reynolds equation on these cell has the same form as eq. (35) and the pressure marked with "○" carry boundary conditions.

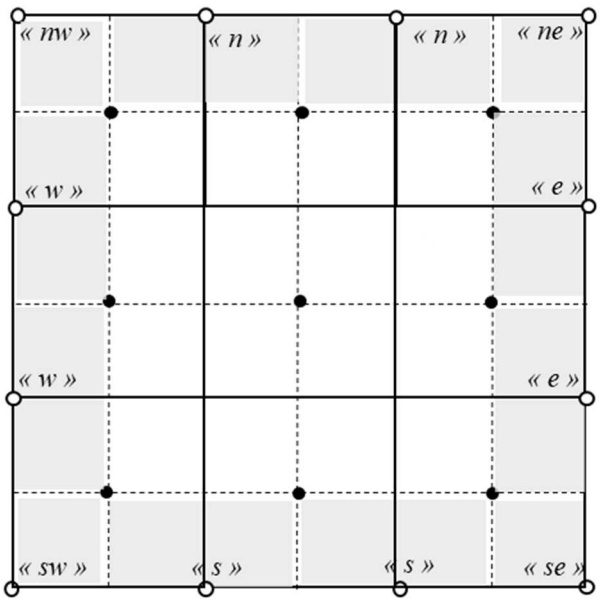

Figure 5. Boundary cells of the dual coarse grid

The discretized eq. (35) is non-linear because its coefficients depend on the unknown pressure on the faces of the basic grid cell. It is therefore solved with a Newton-Raphson algorithm using an

analytically calculated Jacobian. In order to avoid spurious oscillations of the solution or diverging algorithms for high Λ values, the pressures on the *e* and *w* faces of the grid cell are approximated by an "upwind" approach [16], [17], $P_e = P_P$ and $P_w = P_W$ while $P_n = (P_N + P_P)/2$ and $P_s = (P_S + P_P)/2$.

In all cases, the solution of the linear systems associated with the Newton-Raphson algorithm on the coarse grid or arising from the discretization of eqs. (20) for the homogenization method or of eqs. (26) and (31) is solved with the Pardiso algorithm [*18*].

Numerical results

Numerical results are obtained for the 2D inclined slider depicted in Figure *6*. The lower surface is a flat wall sliding in x direction with velocity U. The upper surface is the wall carrying an irregular surface. The inlet, exit and the lateral surfaces of the domain carry the same constant pressure boundary conditions, P_a.

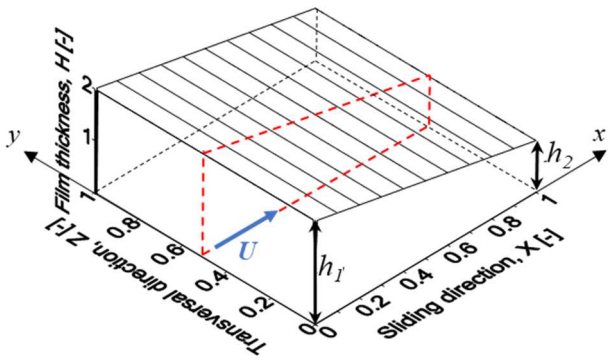

Figure 6. The 2D inclined slider; the upper surface is irregular

The generation of the irregular film thickness starts with a flat upper wall inclined from the left hand side (inlet plane) to the right hand side (outlet plane); the film thickness of the outlet and inlet sections are h_2 and $h_1 = 2h_2$, respectively. The sliding and the transversal distances have the same length L and $h_2/L = 10^{-3}$.

There are many algorithms in the literature for generating an irregular surface [19]. The algorithm given [20] in enables the control of the power spectral density and of the surface heights distribution and was therefore used. In the present analysis, the height of the surface follows a Weibull distribution with a shape parameter of 3. This is considered to be very close to a normal distribution. The power spectrum of the surface heights corresponds to an isotropic autocorrelation length of $2.5\%L$. With these two information (height distribution and power spectrum) and with ISEED=1[2] for the height distribution, the algorithm described in [20] generates the surface heights in 257x257 points of the xy plane. These surface heights have zero mean and unit standard deviation. They are then scaled with a standard deviation $\sigma = 20\%h_2$ and are added to the inclined top surface described by h_1 and h_2. A surface plot is depicted in Figure *7* and shows the irregular character of the film heights progressing from a mean dimensionless inlet height $\bar{h}_1 = 2$ toward an mean exit height $\bar{h}_2 = 1$.

[2] Used in the random number generation subroutine of IMSL[21].

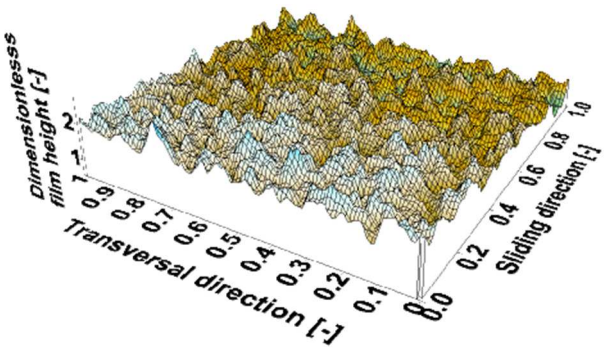

Figure 7. Surface plot of the dimensionless film heights

Reference results were obtained from the direct numerical solution of the Reynolds equation (3) on a fine mesh of 1024 equally spaced control volumes in each direction. Figure 8 depicts the dimensionless load capacity of the 2D slider obtained by integrating the pressures:

$$W = \int_0^1 \int_0^1 (P^* - 1) d\bar{x} d\bar{y} \qquad (37)$$

Due to compressibility, the load tends to an asymptotic value. As shown in Figure *8* the regime characterized by $\Lambda = 1000$ corresponds to a strong compressible regime and the load is close to an asymptotic value. A value of $\Lambda = 10$ corresponds to a mild compressible regime while flow regimes with $\Lambda < 1$ are virtually incompressible.

In the following, the pressures $\bar{P}^*$ obtained by solving Reynolds eq. (3) on the fine grid for $\Lambda = 10$ and 1000 will be considered as reference values for characterizing the results of the homogenization and the multiscale methods. For example, Figure 9 depicts the surface plot of the dimensionless pressures for these two values of Λ.

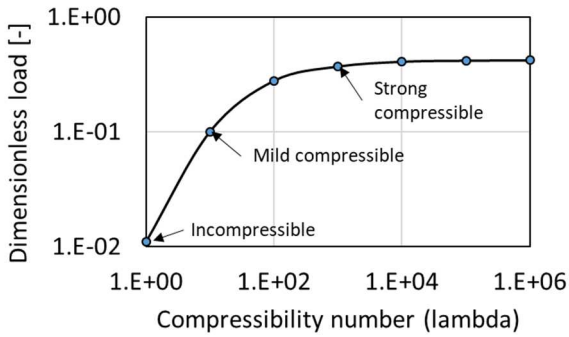

Figure 8. Dimensionless load of the compressible 2D slider ($h_1 = 2h_2$, $L = B$)

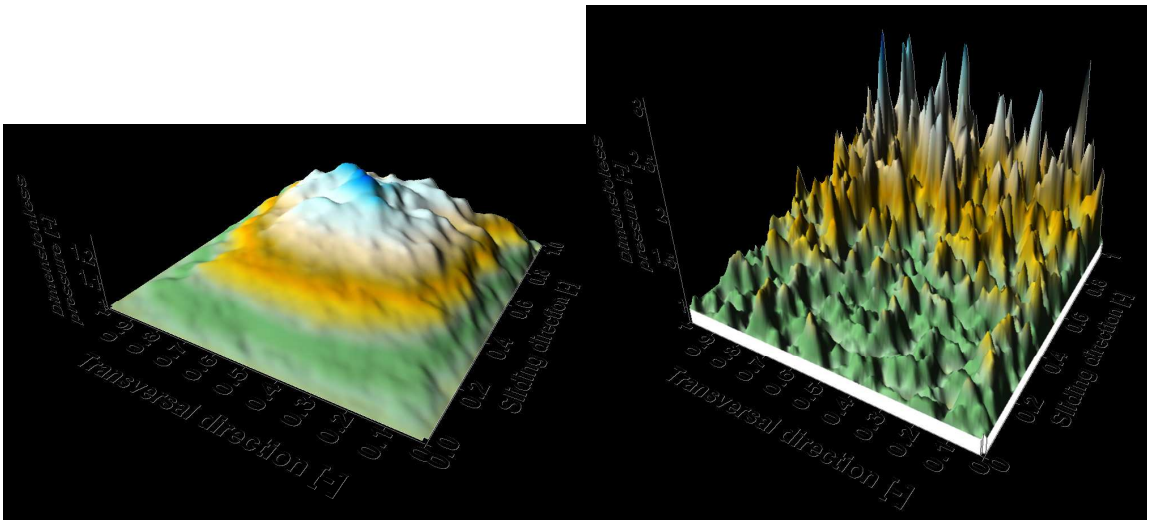

Figure 9. Surface plot of the dimensionless pressure

Three computational grids were used for the homogenization and the multiscale method: 32x8, 64x8 and 128x8 equally spaced control volumes in each direction. The first grid had N_{xCG}=N_{yCG}=32 CV in the coarse grid and N_{xFG}=N_{yFG}=256 CV of the fine grid corresponding to the nodes used for generating the film heights. The last grid had N_{xCG}=N_{yCG}=128 CV in the coarse grid and N_{xFG}=N_{yFG}=1024 CV of the fine grid corresponding to the discretization cells used for obtaining the reference solution P^*.

Figure 10 depicts the pressure variation in the mid-plane of the 2D slider for a mild compressible regime ($\Lambda = 10$) along the interrupted line contour depicted in Figure 6. This kind of presentation was preferred to surface plots for the visual inspection of the results. The dots correspond to the results on the coarse grid while the interrupted line corresponds to the results on the fine grid obtained by using eqs. (5), (19) and $\varepsilon = 1/N_{xCG}$ (or N_{yCG}) for the homogenization method and eq. (30) for the multiscale method.

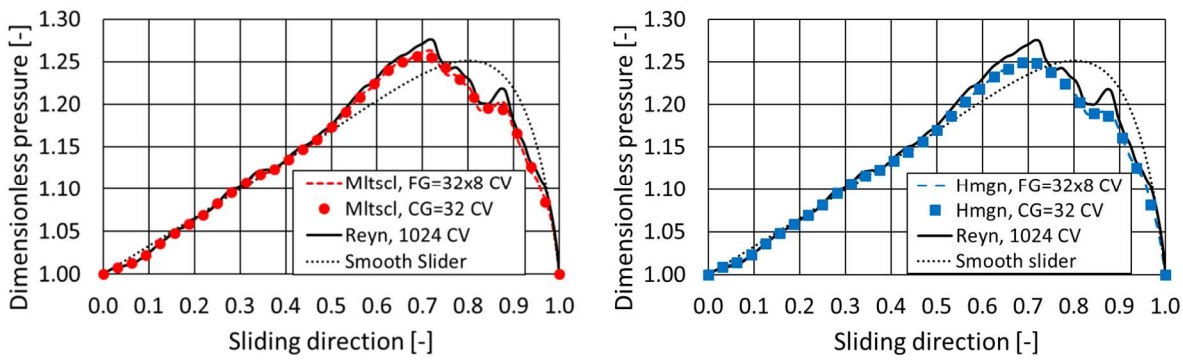

Figure 10. Pressure variation in the mid-plane of the 2D slider ($\Lambda = 10$, CG=32 CV, FG=32x8 CV)

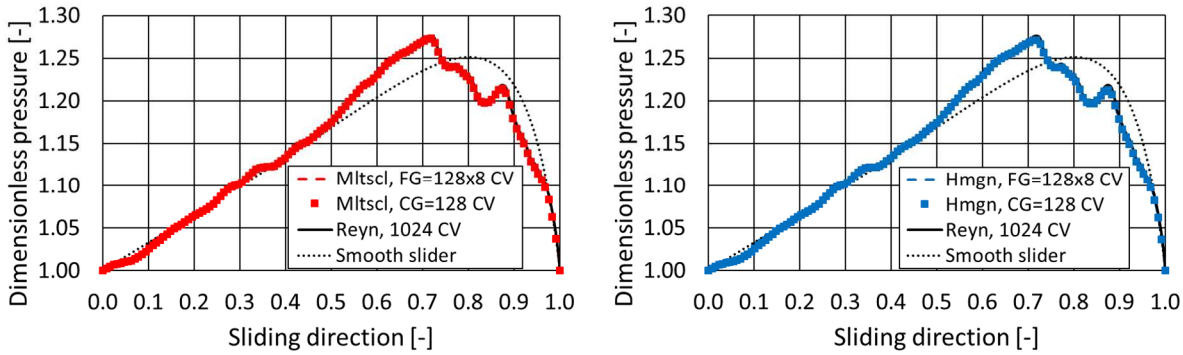

Figure 11. Pressure variation in the mid-plane of the 2D slider ($\Lambda = 10$, CG=128 CV, FG=128x8 CV)

Figure 11 depicts the same pressure variation for $\Lambda = 10$ but for $N_{xCG} = 128$. The results coincide with the reference solution P^*. The accuracy is also enlightened by the error between the homogenized (or the multiscale) results and the reference values.

$$error = \frac{1}{N_{xCG,FG}} \sqrt{\sum (P - P^*)^2} \quad (38)$$

Table 1 shows that the errors for the homogenization and the multiscale methods are very much the same, either on the coarse, or on the fine grid. The errors are one or two orders of magnitude smaller on the fine grid compared to the coarse grid. If depicted in logarithmic coordinates both the coarse and the fine grid errors would show a linear decrease with the grid density.

Table 1 Accuracy of the homogenization and multiscale methods relative to the reference solution

$N_{x,y}$	Lambda=10 (mild compress.)				Lambda=1000 (strong compress.)			
	Coarse Grid (CG)		Fine Grid (FG)		Coarse Grid (CG)		Fine Grid (FG)	
	Hmgn	Mltscl	Hmgn	Mltscl	Hmgn	Mltscl	Hmgn	Mltscl
32x8	2.01E-3	1.39E-3	6.66E-4	3.92E-4	1.84E-2	1.72E-2	8.35E-3	1.39E-2
64x8	7.17E-4	4.63E-4	2.50E-4	1.56E-4	9.60E-3	8.77E-3	3.74E-3	4.26E-3
128x8	2.27E-4	1.60E-4	7.87E-5	5.46E-5	3.72E-3	3.40E-3	1.36E-3	1.40E-3

The results for the strong compressible regime, $\Lambda = 1000$, are depicted in Figure 12 and Figure 13. The pressure variations are much more rapid than for the mild-compressible regime, therefore, as shown in Table 1, the errors obtained with the same grid densities are larger. Figure 12 depicts the results on the coarse grid (left) and on the fine grid (right) for $N_{x,yCG} = 32$. The results obtained with the homogenization and the multiscale method on the coarse grid are close (Figure 12, left). This is not the case for the results estimated on the fine grid (Figure 12, right) were the homogenization method underestimates the reference values, while the multiscale method overestimates them. However, Figure 13 obtained for $N_{x,yCG} = 128$ shows that when the errors on the coarse grid are reduced then the estimations on the fine grid raise no problems.

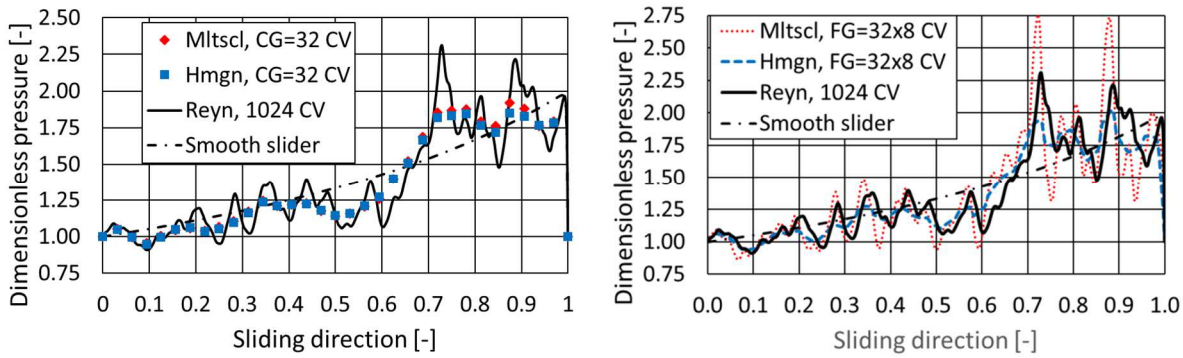

Figure 12. Pressure variation in the mid-plane of the 2D slider ($\Lambda = 1000$, CG=32 CV, FG=32x8 CV)

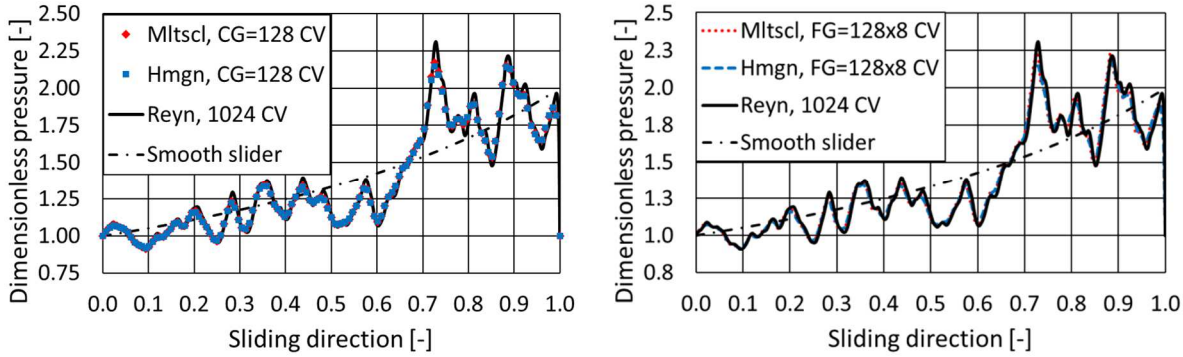

Figure 13. Pressure variation in the mid-plane of the 2D slider ($\Lambda = 1000$, CG=128 CV, FG=128x8 CV)

The accuracy of both methods for $\Lambda = 10 \ldots 1500$ and for the mid-plane pressures is depicted in Figure 14. The accuracies of the two methods are very close excepting the results obtained with the multiscale method on the fine grid FG=32x8 CV. This finding is consistent with the results depicted on the right part of Figure 12 showing large variations of the multiscale pressure on the fine grid. The conclusion is that 32 CV of the coarse grid are not sufficient for the multiscale method for obtaining a good enough solution on the fine grid starting with $\Lambda = 500$. For higher coarse grid densities, the accuracy of the two methods is similar.

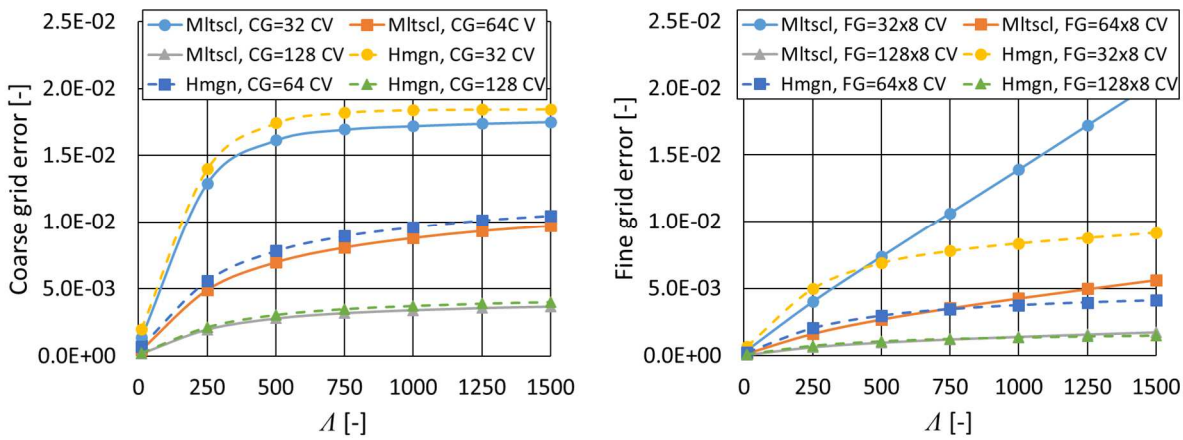

Figure 14. Errors of the pressure variation in the mid-plane of the 2D slider (coarse grid-left, fine grid-right)

The relative errors for the load and the friction force of the slider calculated with the homogenization and the multiscale methods with respect to the reference results are depicted in Figure 15. In all cases, the density of fine grid is N_{xCG}x8. The relative errors are comprised between 10^{-1} and 10^{-2} or

less with lower values for the multiscale method although the differences between the two methods are not significant. However, the results depicted in Figure 14 and in Figure 15 show that relative errors of the order of 10^{-2} can not be obtained with the coarse grid of 32 CV and in this case higher coarse grid densities should be privileged for $\Lambda > 500$.

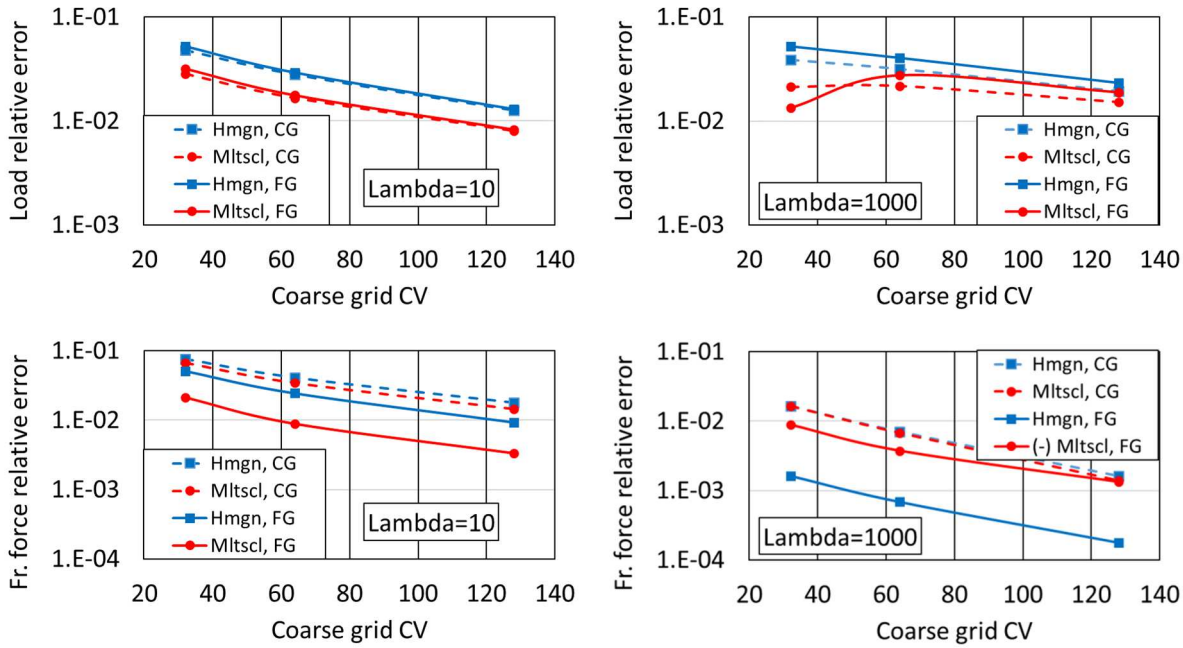

Figure 15. Relative error of the load and friction force (the density of the fine grid is 8 times the density of the coarse grid)

The computational effort required by the homogenization and multiscale method is depicted in Figure 16a,b. The computational effort is here measured by the ratio between the CPU time required for a full solution divided by the CPU time of the full Reynolds equation on the same grid. The CPU function was preferred to the SYSTEM_CLOCK function because the latter depends on the number of threads used. Indeed, both the homogenization and the multiscale method can be easily parallelized with the OMP option. This is an important advantage because the local solutions on the fine grid described either by eqs. (20) or by eqs. (26) and (31) can be dispatched on many threads. However, the result of CPU function is independent of the number of threads. Figure 16a shows the ratio CPU/CPU(Reyn1024) for different grid densities. The homogenization method is slightly more efficient because it requires the solution of four discretized eqs. (20) on the local fine grid instead of five eqs. (26) and (31) for the multiscale method. However, the difference is small. The ratio increases to 30…40% of CPU(Reyn1024) with the density of the fine grid. However, a fine grid density of 1024^2 cells is not large and Figure 16b shows that smaller CPU ratios are obtained when increasing the fine grid density. The homogenization and the multiscale methods have a net advantage in terms of CPU for very large size fine grids (two orders of magnitude reduction for the 4096^2 fine grid) when the numerical solution of the full Reynolds equation must use the hard memory for solving the linear system.

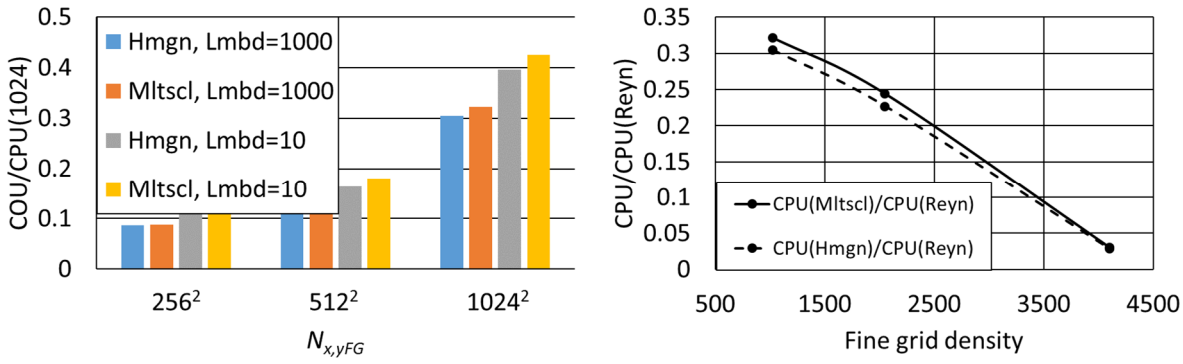

Figure 16. Computational effort of the homogenization and multiscale methods relative to the reference solution of the Reynolds equation

Another point under discussion is the accuracy of the reconstructed solution on the fine grid when the coarse grid discretization has different number of cells in x and y direction. For the multiscale method, eq. (30) operates on all kind of coarse grids but this can raise questions for the homogenization methods. Indeed, the key point for the reconstruction of the fine grid solution of the homogenization method is the definition of the small parameter $\varepsilon = 1/N_{CG}$ in eq. (5). This raises no problem when $N_{xCG} = N_{yCG}$ but is not well defined if $N_{xCG} \neq N_{yCG}$. A heuristic approach case would be:

$$\varepsilon = 1/\sqrt{N_{xCG} N_{yCG}} \qquad (39)$$

This is verified in the following. The accuracy of the results obtained with different coarse grids is given in Table 2. Different N_{xCG} and N_{yCG} were combined but the resulting fine grid always had a density of 1024 cells. There is a very slight increase of the error given by the homogenization method compared to the multiscale method but the difference is quite small and shows that the heuristic eq. (39) for reconstructing the fine grid solution of the homogenization method performs very well.

Table 2 Accuracy of the homogenization and multiscale methods relative to the reference solution ($N_{xCG} \neq N_{yCG}$ and $N_{xFG}=N_{yFG}=1024$)

N_x	N_y	Lambda=10 (mild compress.)				Lambda=1000 (strong compress.)			
		Coarse Grid (CG)		Fine Grid (FG)		Coarse Grid (CG)		Fine Grid (FG)	
		Hmgn	Mltscl	Hmgn	Mltscl	Hmgn	Mltscl	Hmgn	Mltscl
128/8	*128/8*	*2.27E-4*	*1.60E-4*	*7.87E-5*	*5.46E-5*	*3.72E-3*	*3.40E-3*	*1.36E-3*	*1.40E-3*
128/8	64/16	3.10E-4	1.76E-4	1.10E-4	5.94E-5	5.13E-3	4.21E-3	1.84E-3	1.69E-3
128/8	32/32	4.61E-4	2.49E-4	1.61E-4	8.38E-5	8.35E-3	7.07E-3	2.94E-3	2.51E-3
64/16	128/8	5.86E-4	4.34E-4	1.43E-4	1.04E-4	8.60E-3	8.09E-3	2.38E-3	2.39E-3
64/16	*64/16*	*6.78E-4*	*4.68E-4*	*1.67E-4*	*1.12E-4*	*9.66E-3*	*8.77E-3*	*2.64E-3*	*3.02E-3*
64/16	32/32	8.64E-4	5.50E-4	2.12E-4	1.29E-4	1.26E-2	1.14E-2	3.40E-3	3.83E-3
32/32	128/8	1.61E-3	1.25E-3	2.65E-4	1.93E-4	1.61E-2	1.59E-2	3.88E-3	3.77E-3
32/32	64/16	1.67E-3	1.36E-3	2.74E-4	2.04E-4	1.64E-2	1.61E-2	3.92E-3	4.41E-3
32/32	*32/32*	*1.86E-3*	*1.41E-3*	*3.01E-4*	*2.01E-4*	*1.83E-2*	*1.72E-2*	*4.30E-3*	*7.03E-3*

Summary and conclusions

The present work compares the homogenization and the multiscale methods applied to the compressible Reynolds equation in a very narrow channel with rough (irregular) walls. The article details all the stages of development of the homogenization method and underlines that under

certain conditions the local problems have the same formulation as for an incompressible fluid. This treatment of local problems greatly simplifies the resolution. Then the multiscale method inspired from porous media flow is adapted for taking into account the Couette part of the flow. This extension of the algorithm is not present in the literature. According to the homogenization method, the local problem is then treated as for an incompressible fluid.

Examples of the numerical solutions are given for a convergent, two-dimensional narrow slider with a realistic, irregular gap height typical for gas lubrication problems. The results were compared with the solution of the original Reynolds equation.

Several points were analyzed: the influence of the density of the coarse mesh, the precision of the solution obtained on the fine mesh and the computational effort. The results obtained for mild and strong compressible regimes showed that the two methods are very similar in terms of accuracy and computational effort. One could underline that the multiscale method has a slight advantage in terms of accuracy while the computational effort of the homogenization method is slightly less but these differences are quantitatively not important.

Both methods worked well for this realistic calculation case compared to the original Reynolds equation. This was to be expected for the multiscale method that has no *a priori* limitations in terms of irregularity of its coefficients or on the number of coarse grid cells in x and y directions. The results obtained with the homogenization method were also accurate both on the coarse mesh and on the fine mesh, although the irregular channel height had not an exact periodic pattern. The heuristic equation used to define the small parameter ε when the coarse grid has different x and y densities works well for obtaining the solution on the fine grid.

Within the limits of the simplifying assumptions given in the introduction, the two methods are equivalent. What could make the difference in the future is the ease of integrating additional non-linear effects such as taking into account sporadic contacts between asperities or the superposition of a temperature field.

Nomenclature

$A_{0,1,2}$, $A'_{0,1,2}$,	operators defines by eqs. (9)-(14)
A_{ij},	coefficient of the homogenized eq. (22) or of the multi-scale eq. (36)
B,	width of the domain of analysis, [m]
C_i, D,	coefficients of the multi-scale Reynolds eq. (39)
h,	thin film thickness (gap height), [m]
h_m,	average film height, [m]
h_{min},	minimum gap height, [m]
h_1, h_2,	inlet and exit height of the inclined slider
L,	length of the domain of analysis, [m]
$\dot{m}$,	local mass flow rate, [kg/m/s]
P,	pressure, [Pa]
P^*,	reference solution for pressure, [Pa]
$\hat{P}$,	approximation of the pressure in the multi-scale method, [Pa]

P_a,	atmospheric pressure, [Pa]
q,	local flow rate, [m^2/s]
U,	wall velocity, [m/s]
$\bar{W}$,	dimensionless load
x, y,	distances, [m]
σ,	standard deviation of gap height, [m]
μ,	dynamic viscosity, [Pas]
Λ,	compressibility number
ε,	small parameter (ratio of the short and long length scale)
Ω,	domain of analysis
ϕ_i,	shape functions used in the multi-scale method
χ_i,	functions used in the homogenization method and defined by eq. (20)

Indice:

0, 1,	long and short length scales
eq,	equivalent
x, y,	axis of the coordinate system

References

[1] Hansen J., Bjorlong M., Larsson, R. A New Film Parameter for Rough Surface EHL Contacts with Anisotropic and Isotropic Structures. Tribology Letters 2021; 69:37.

[2] Bhushan B. Principles and Applications of Tribology 2nd Edition 2013, John Wiley & Sons, Ltd.

[3] Patir N., Cheng H.S. An Average Flow Model for Determining Effects of Three-Dimensional Roughness on Partial Hydrodyanmic Lubrication. J Lubric Tech 1978; 100(1):12-17.

[4] Bayada G., Chambat M. New Models in the Theory of the Hydrodynamic Lubrication of Rough Surfaces. J Tribol 1988; 110(3): 402-407.

[5] Almqvist A., Dasht J. The homogenization process of the Reynolds equation describing compressible liquid flow. Tribol Int 2006; 39(9): 994-1002.

[6] Sahlin F., Almqvist A., Larsson R., Glavatskih S. Rough surface flow factors in full film lubrication based on a homogenization technique. Tribol Int 2007; 4(7): 1025-1034.

[7] Fatu A., Bonneau D., Fatu R. Computing hydrodynamic pressure in mixed lubrication by modified Reynolds equation. Proc. IMechE Part J J Eng Tribol 2012; 226(12): 1074-1094.

[8] Buscaglia G.C., Jai M. Homogenization of the Generalized Reynolds Equation for Ultra-Thin Gas Films and Its Resolution by FEM. J. Tribol. 2004; 126 (3): 547-552.

[9] Jai M. Homogenization and two-scale convergence of the compressible Reynolds lubrication equation modelling the flying characteristics of a rough magnetic head over a rough rigid-disk. Modélisation mathématique et analyse numérique 1995; 29(2): 199-233.

[10] Almqvist A., Fabricius J., Wall P. Homogenization of a Reynolds equation describing compressible flow. J Math Anal Appl 2012; 390(2): 456-471

[11] Rom M., Konig F., Muller S. , Jacobs G. Why homogenization should be the averaging method of choice in hydrodynamic lubrication. Applications in Engineering Science 2021; 7(9): 100055.

[12] Yildiran I. N., Temizer I., Cetin B. Homogenization in Hydrodynamic Lubrication: Microscopic Regimes and Re-Entrant Textures. J Tribol 2018; 140(1): 011701.

[13] Hou T. Y., Wu, X.-H. A Multiscale Finite Element Method for Elliptic Problems in Composite Materials and Porous Media. J. Comp Phys 1997; 134(1): 169-189.

[14] Jenny P., Lee S. H., Tchelepi H. A. Multi-scale finite-volume method for elliptic problems in subsurface flow simulation. J Comp Phys 2003; 187(1): 47-67.

[15] Lunati I., Jenny P. Multiscale finite-volume method for compressible multiphase flow in porous media. J Comp Phys 2006; 216(2): 616-636.

[16] Arghir M., Le Lez S., Frêne J. Finite volume solution of the compressible Reynolds equation - linear and non linear analysis of gas bearings. Proc. IMechE Part J J Eng Tribol 2006; 220(7): 617-627.

[17] Faria M. T. C., San Andrés L. On the Numerical Modeling of High-Speed Hydrodynamic Gas Bearings. J. Tribol 2000; 122(1):124-130.

[18] Schenk O., Gartner K. Solving unsymmetric sparse systems of linear equations with PARDISO. Future Gener Comp Sy 2004; 20(3): 475-487.

[19] Pawlus P., Reizer R., Wieczorowski M. A review of methods of random surface topography modeling. Tribol Int 2020; 152 (12): 106530.

[20] Pérèz-Ràfols F., Almqvist A. Generating randomly rough surfaces with given height probability distribution and power spectrum. Tribol Int 2019; 131(3); 591-604.

[21] IMSL® Fortran Subroutines for Mathematical Applications Volumes 1 and 2, Copyright 1997, by Visual Numerics, Inc.

Appendix

The coefficients $A_{ne/j,i}$ obtained after injecting eq. (30) in the fluxes given by eq. (32) are:

$$A_{ne/1,i} = -\int_{x_{ne}}^{x_{nee}} h^3 \frac{\partial \phi_i}{\partial y} dx\,, \qquad A_{ne/1,5} = -\int_{x_{ne}}^{x_{nee}} h^3 \frac{\partial \phi_5}{\partial y} dx$$

$$A_{ne/2,i} = -\int_{y_{ne}}^{y_{nne}} h^3 \frac{\partial \phi_i}{\partial x} dy\,, \qquad A_{ne/2,5} = -\int_{y_{ne}}^{y_{nne}} h^3 \frac{\partial \phi_5}{\partial x} dy + \Lambda \int_{y_{ne}}^{y_{nne}} h dy \qquad (40)$$

$$A_{ne/3,i} = -\int_{x_n}^{x_{ne}} h^3 \frac{\partial \phi_i}{\partial y} dx\,, \qquad A_{ne/3,5} = -\int_{x_n}^{x_{ne}} h^3 \frac{\partial \phi_5}{\partial y} dx$$

$$A_{ne/4,i} = -\int_{y_e}^{y_{ne}} h^3 \frac{\partial \phi_i}{\partial x} dy\,, \qquad A_{ne/4,5} = -\int_{y_e}^{y_{ne}} h^3 \frac{\partial \phi_5}{\partial x} dy + \Lambda \int_{y_e}^{y_{ne}} h dy$$

for $i = \overline{1,4}$. These definitions hold for the control volume ne of the dual grid detailed in Figure 3. The coefficients for the control volumes nw, sw, se of the dual grid depicted in Figure 2a are obtained in a similar manner.